Precision CMG Control for High-Accuracy Pointing

SAM P. LIDEN*
Sperry Flight Systems, Phoenix, Ariz.

Extremely precise gimbal control, as is necessary for CMG (Control Moment Gyro) high-accuracy-pointing control systems, is obtainable and has been demonstrated for large single-gimbal CMGs. A proportional-plus-integral control law, where the integral gain is substantially greater than the gradient of the gimbal "stiction" profile, makes possible wide bandwith control of gimbal rate at extremely low levels. The stiffness of structures between the rotor rim and the vehicle in the CMG output axis should be substantially greater than the integral gain in order to maintain control-loop stability with the relatively high gain required. A bandwidth of 20 Hz at 0.005°/sec gimbal rate, producing 0.05 ft-lb output torque, has been demonstrated for a 600 ft-lb-sec CMG. This unit also produced 100 ft-lb output torque at 10°/sec gimbal rate, demonstrating a dynamic range in output torque of at least 2000 : 1. Further improvement is feasible.

Introduction

THE pointing accuracy obtainable with CMG attitude control systems is limited, as far as the CMGs are concerned, principally by 1) the vibrations induced by the CMGs and 2) the level of control precision provided by the gimbal control system. This paper addresses the second problem.

Since reaction wheels, single-gimbal CMGs and double-gimbal CMGs are all controlled via some type of torque motor, it is sometimes erroneously assumed that all three types of momentum exchange devices have approximately the same dynamic range (ratio of maximum to minimum controllable output) in the output torque, being limited by the dynamic range of the torque motor. A combination of large CMGs and small reaction wheels has therefore been proposed[1-3] for systems that require large torque or angular momentum capacity as well as very precise torque control. In the case of single-gimbal CMGs, however, and to a lesser degree for double-gimbal CMGs, when the output torque is controlled by controlling gimbal rate, it is possible to control the gimbal within the friction breakaway zone of the gimbal pivot, thereby greatly extending the dynamic range of the output torque at the lower end.

This paper is concerned principally with design of gimbal-rate control systems for single-gimbal CMGs that are required to maintain wide bandwidth control at extremely low levels of gimbal-rate command signals. Discussion on double-gimbal CMGs is presented in a following paragraph. Test data obtained on a Sperry 600 ft-lb-sec single-gimbal CMG, shown in Fig. 1, are also presented.

Fig. 1 Sperry 600 ft-lb-sec single-gimbal CMG.

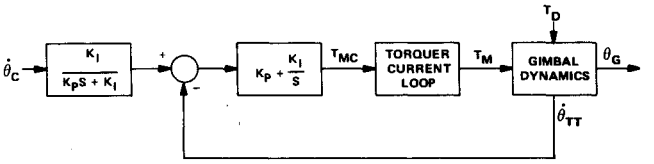

Fig. 2 Undetailed gimbal-rate control loop.

Gimbal-Rate Control Law

An undetailed block diagram of a gimbal-rate control system, identifying the major dynamic elements and the recommended control law, is given in Fig. 2. The rate $\dot{\theta}_G$ of the angular momentum vector about the gimbal axis is to be controlled to equal a commanded gimbal rate $\dot{\theta}_C$. The rate of the tachometer $\dot{\theta}_{TT}$ is not precisely the same as $\dot{\theta}_G$, however, because of compliances in the structures. The effects of such compliances will be considered later on. A current control loop is employed for each phase of the torque motor (direct-drive brushless DC) to produce motor torque T_M closely equal to commanded motor torque T_{MC}. It employs lead-lag compensation, with the zero cancelling the pole associated with the motor electrical time constant, and can typically achieve bandwidth above 500 Hz with high gain and phase margins.

Consider first an idealized model of the gimbal control system shown in Fig. 3 for the purpose of later comparisons with more realistic models. The current loops are assumed to have unity gain, and the torquer and tachometer have no anomalies. In addition, the model used here for gimbal dynamics includes only low-frequency characteristics and is simply equivalent to an inertia† I_{GE} which is greater than the actual gimbal inertia I_G. It is given by

$$I_{GE} = I_G + (H^2/K_O) \tag{1}$$

where H is the CMG angular momentum and K_O is the over-all stiffness of the series of structures between the rotor rim and the spacecraft, including the CMG mounting structures about the CMG output axis. This model yields the following closed loop transfer functions:

$$\frac{\theta_G}{\theta_1} = \frac{(K_P/K_I)s+1}{(s^2/\omega_n^2)+2\zeta(s/\omega_n)+1} \tag{2}$$

Presented as Paper 72-1076 at the AIAA Guidance and Control Conference, Key Biscayne, Fla., August 20–22, 1973; submitted September 6, 1973; revision received December 14, 1973.
Index category: Spacecraft Attitude Dynamics and Control.

* Principal Engineer, Satellite Control Products. Member AIAA.

† "Inertia" denotes "moment of inertia" throughout this paper.

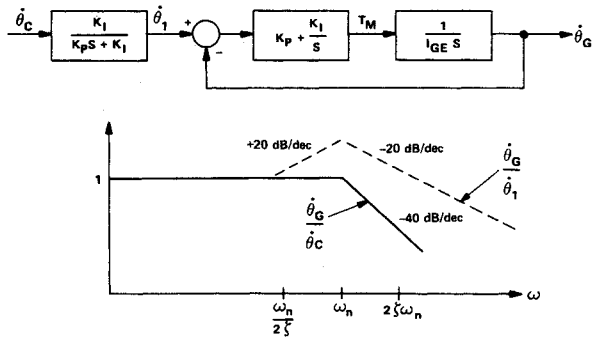

Fig. 3 Idealized gimbal-rate control loop.

$$\frac{\dot{\theta}_G}{\dot{\theta}_C} = \frac{1}{(s^2/\omega_n^2)+2\zeta(s/\omega_n)+1} \tag{3}$$

where

$$\omega_n = (K_I/I_{GE})^{1/2} \tag{4}$$

and

$$\zeta = K_P/2\omega_n I_{GE} \tag{5}$$

K_I and K_P may then be selected to provide the desired bandwidth and damping ratio. Equations (2) and (3), and the corresponding asymptotic gain plots shown in Fig. 3, illustrate the effect of the prefilter: it simply cancels the zero in $\dot{\theta}_G/\dot{\theta}_1$ to provide a flat response curve, a faster roll-off (−40 db/decade) at high frequencies, and to eliminate a possible false impression of an underdamped control loop. It may be considered to be part of the vehicle control loop compensation, and can easily be modified or eliminated, if desired, without affecting the dynamics of the gimbal control loop.

Effect of Gimbal Friction

Tests have shown that for small displacements the gimbal friction torque (resistance to motion) acts as a spring, that is, the restoring torque is approximately proportional to displacement. Figure 4 shows a typical torque vs gimbal displacement curve obtained for the tested CMG which incorporates a brushless torquer and a brush-type tachometer. The spring-like restoring torque, in the cases of brush and bearing friction, is explainable in terms of the compliant displacements in the brush supporting structures and the bearing balls which take place before breakaway occurs. In the case of motor hysteresis drag torque, it is explainable in terms of a low-level "permanent" magnetism produced in the stator by the highly magnetized rotor, tending to maintain the rotor stationary. It is significant that this spring-like restoring torque is continuous and linear through zero, i.e., it does not exhibit deadzone or step characteristics. Dahl[4] came to the same conclusion in modeling roller bearing and solid sliding friction. Continuous control of the gimbal is therefore possible within the spring region of the gimbal friction profile by over-

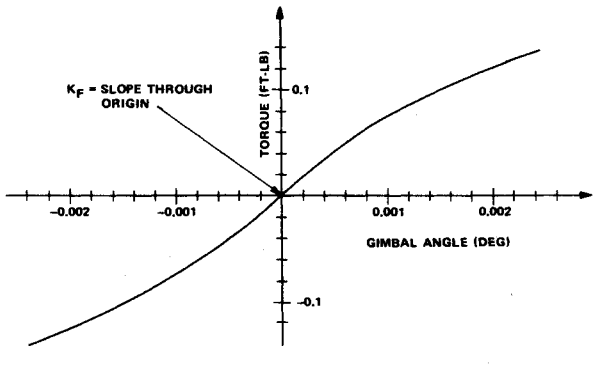

Fig. 4 Gimbal friction profile for small displacements.

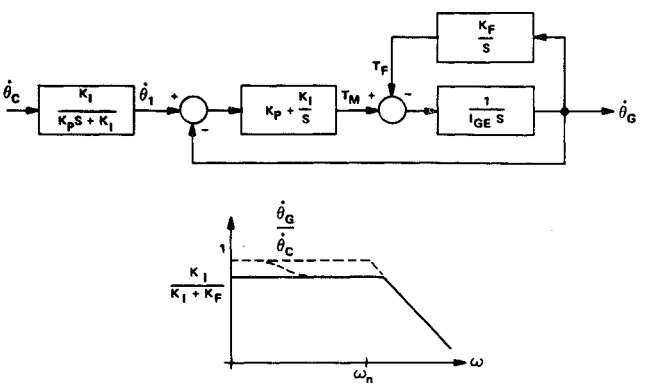

Fig. 5 Effect of gimbal friction for low levels of gimbal rate.

powering the friction spring with high integral gain in the control loop.

To show how this is achieved, consider the model in Fig. 5. By the addition of a model for the restoring torque T_F, equal to $K_F\theta_G$, the case where the gimbal displacement is very small is simulated. The over-all transfer function then is given by

$$\frac{\dot{\theta}_G}{\dot{\theta}_C} = \left(\frac{K_I}{K_I+K_F}\right)\frac{1}{\frac{I_{GE}}{K_I+K_F}s^2+\frac{K_P}{K_I+K_F}s+1} \tag{6}$$

The asymptotic gain plot shown in Fig. 5 illustrates the effect of K_F. Note that the gain is reduced by $K_I/(K_I+K_F)$, and the break frequency is not reduced. As long as K_I is considerably greater than K_F, bandwidth is not sacrificed at low gimbal-rate amplitudes, no matter how low they are. No low-level threshold therefore, will exist due to gimbal friction. Low-level performance is instead expected to be limited by noise and electronic bias.

Since the amplitude of the sinusoidal gimbal displacement is inversely proportional to frequency for a sinusoidal rate of a given amplitude ($\theta = \dot{\theta}/\omega$), the gimbal displacement amplitude increases as the frequency is decreased. At some frequency, as the frequency is decreased, the displacement amplitude will start breaking out of the friction spring region, and as frequency continues to decrease, the friction torque becomes mainly the constant coulomb friction (which is compensated for by the control-law integrator) and will have less effect on the gain. The transition region where the gain changes from 1 to $K_I/(K_I+K_F)$ (see Fig. 5), therefore, moves down in frequency as the amplitude of the gimbal rate signal decreases, accounting for the loss in bandwidth that is observed at low gimbal rate amplitudes when $K_I/(K_I+K_F) \ll 1$. Figure 6 illustrates this situation.

For the 600 ft-lb-sec CMG tested as described later on, the value of K_F was approximately 3000 ft-lb/rad with the wheel running. By selecting K_I = 10,000 ft-lb/rad the gain reduction at low levels is then no more than 2.3 dB, and for K_I = 25,000 ft-lb/rad the gain reduction is less than 1 dB.

Since the gimbal control-loop bandwidth (Eq. 4) depends on K_I, its value is likely to be dictated by the low-level performance

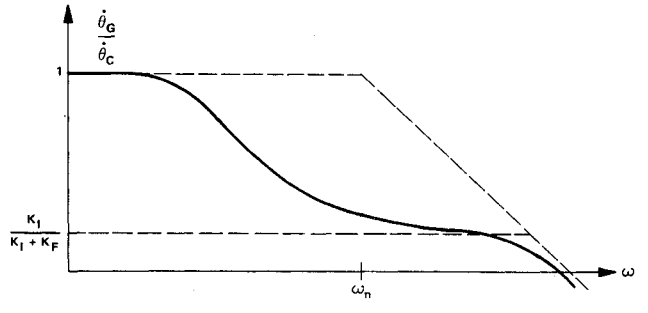

Fig. 6 Low-level response for $K_I \ll K_F$.

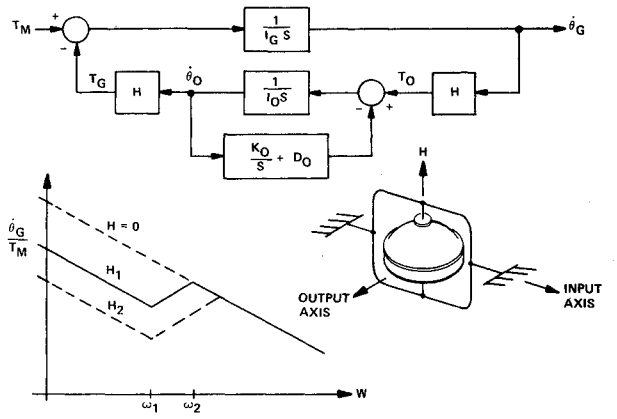

Fig. 7 Model with lumped output-axis inertia.

criterion ($K_I \gg K_F$), and may yield a higher bandwidth than is required for the CMG attitude control actuator system.

Effect of Structural Compliance

Compliances in the CMG and in the CMG mounting structures have been found to limit the level of gimbal loop gain possible, and may therefore prevent the CMG system from achieving the desired low-level response. Analytical models of gimbal control-loop dynamics with compliant structures have not been completely satisfactory in predicting instabilities encountered in hardware testing, but have provided some insight and guidance in achieving the kind of performance described further on. Accurate modeling of CMG structures is difficult because many structures, such as shells, are not well represented by lumped masses and springs; also, many parameters of a high-order model are difficult to identify, and some vary with gimbal position. This discussion is therefore not intended to present precise or representative models of structural dynamics of CMGs but only to describe the reasoning that led to the obtained hardware results.

Consider first a simple model for the output axis compliance to show the effect of equivalent inertia and some of the relations involved. A single lumped inertia I_O is assumed about the output axis which is tied to ground by a spring of stiffness K_O, and a dashpot of damping rate D_O. Figure 7 shows the resulting model for the gimbal dynamics. This model may be interpreted as assuming that all the mass contributing to the output-axis inertia I_O is located in the rotor rim.

The block diagram in Fig. 7 is explained as follows: the net torque activity on the gimbal inertia I_G in the input (gimbal) axis is the motor torque T_M minus the gyroscopic feedback torque T_G. The resulting gimbal rate $\dot{\theta}_G$ results in a gyroscopic torque $T_O = \dot{\theta}_G H$ in the output axis, which is the desired CMG output torque. The net torque acting on I_O is T_O minus the restraining torque of the structural spring and dashpot given by $K_O\theta_O + D_O\dot{\theta}_O$. The resulting output axis rate $\dot{\theta}_O$ results in a gyroscopic torque T_G back into the input axis in a direction that causes $\dot{\theta}_G$ to decrease. The resulting transfer function is

$$\frac{\dot{\theta}_G}{T_M} = \left(\frac{(s^2/\omega_1{}^2)+2\zeta_1(s/\omega_1)+1}{(s^2/\omega_2{}^2)+2\zeta_2(s/\omega_2)+1}\right)\frac{1}{I_{GE}s} \tag{7}$$

where I_{GE} is the equivalent inertia given by Eq. (1) and where the two break frequencies are given by

$$\omega_1 = (K_O/I_O)^{1/2} \tag{8}$$

$$\omega_2 = (K_O/I_O + H^2/I_G I_O)^{1/2} = (I_{GE}/I_G)^{1/2}\omega_1 \tag{9}$$

The low-frequency model assumed in Fig. 3 corresponds to assuming $\omega \ll \omega_1$ in the above model.

Since ω_1 is always less than ω_2, the phase angle of the open-loop transfer function, with the above model for $\dot{\theta}_G/T_M$ (Eq. 7), must lie between $+90°$ and $-180°$. The loop is therefore stable for any $K_I > 0$ and $K_P > 0$. In reality there are, of course, sources of phase lag (the current loop, tachometer, amplifiers) not accounted for in the model, and since structural modes are generally very lightly damped they should be maintained well outside the desired control-loop crossover frequency $2\zeta\omega_n$ [see Eqs. (4) and (5)] where the gain may be reduced by filtering. By maximizing the output axis stiffness K_O, the structural mode frequency ω_2 is maximized, the effective gimbal inertia is minimized (Eq. 1), and the gain at ω_2 is minimized as shown by the gain of the asymptotic plot at ω_2 (see Fig. 7)

$$\frac{1}{I_G\omega_2} = \frac{1}{I_G(K_O/I_O + H^2/I_G I_O)^{1/2}} \tag{10}$$

High output axis stiffness is therefore desirable, but precisely how much is required cannot be established when the model is not precise. If one simply postulates the requirement that the structural mode ω_2 [Eq. (9)] must be much greater than the loop crossover frequency $2\zeta\omega_n$, the following inequality results [from Eqs. (1, 4, and 9)]:

$$K_I \ll \frac{I_{GE}{}^2}{4\zeta^2 I_G I_O}K_O = \frac{I_G}{4\zeta^2 I_O}\left(1+\frac{H^2}{I_G K_O}\right)^2 K_O \tag{11}$$

This inequality can be satisfied for any given values of K_I, H and inertias by making K_O either sufficiently large or sufficiently small. It is satisfied for all K_O if

$$K_I \ll H^2/\zeta^2 I_O \tag{12}$$

[The right-hand side of Eq. (12) is the minimum, with respect to K_O, of the right-hand side of Eq. (11).] For large CMGs, this is not much of a limitation on the permissible integral gain while the wheel is running. A representative value for I_O is 4 ft-lb-sec^2; hence for $H = 600$ ft-lb-sec, $K_I = 25{,}000$ ft-lb/rad easily satisfies Eq. (11) for any K_O.

Hardware testing, however, where the CMG was mounted on a fixture with adjustable output axis stiffness, demonstrated that the integral gain cannot be as high as the above relation would allow for very low output axis stiffness. If K_O is restricted to be above the minimum point (as a function of K_O) of the right-hand side of Eq. (11), then the inequality of this equation becomes

$$K_I \ll (I_G/\zeta^2 I_O)K_O \tag{13}$$

The output axis inertia is generally greater than the input axis inertia, because of the torquer, and ζ^2 is generally selected to be in the vicinity of 0.5. Equation (13) is therefore approximately given by

$$K_I \ll K_O \tag{14}$$

It was concluded that this is a practical guideline for the required relation between K_I and K_O.

Consider now a high-order lumped-parameter model as depicted in Fig. 8 to provide some additional justification for this conclusion. The gimbal torquer acts on the base ring I_{BI} and on the torquer-tachometer rotor I_{TT}, generating a rate $\dot{\theta}_{TT}$ between these bodies which is the controlled variable of the gimbal control loop. The motor torque, transmitted through K_S and K_{WI}, causes the wheel to turn at the rate $\dot{\theta}_{WI}$ around the input axis, resulting in a gyroscopic reaction torque $T_{GO} = -H\dot{\theta}_{WI}$ produced by the wheel on the CMG gimbal about its output axis. This torque, which is transmitted through springs K_{WO}, K_{GO}, and K_{BO} to the spacecraft as the desired output torque, also causes the wheel to turn about its output

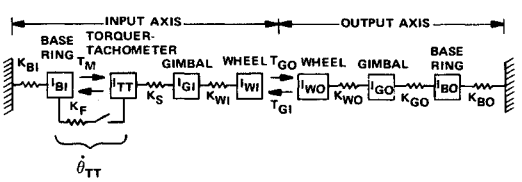

Fig. 8 Higher-order lumped-parameter model for gimbal dynamics.

axis at a rate $\dot{\theta}_{WO}$. Although this rate is small, being constrained by the output-axis structures, it results in a gyroscopic reaction torque $T_{GI} = -H\dot{\theta}_{WO}$ back into the input axis, acting in a direction to oppose $\ddot{\theta}_{WI}$. To model the low-level case, where the gimbal friction torque acts as a restraining spring, a spring K_F is inserted between I_{BI} and I_{TT}. A portion of the friction torque should act on I_{GI}, but the assumed simplification is judged to be of minor significance.

Table 1 lists representative model parameter values for a Sperry CMG mounted on a compliant structure. Relatively soft springs, K_{BI} and K_{BO}, are chosen for the structures holding the CMG base ring to ground to permit some evaluation of the effect of isolation pads and also of a double-gimbal CMG with equivalent stiffness in the orthogonal gimbal control loop (discussed later on).

Table 1 CMG model parameters

Inertias (ft-lb-s^2)		Springs ($\times 10^6$ ft-lb/rad)	
I_{BI}	0.75	K_{BI}	0.14
I_{TT}	0.02	K_F	0.003
I_{GI}	0.9	K_S	2.2
I_{WI}	1.2	K_{WI}	2.5
I_{WO}	1.2	K_{WO}	2.5
I_{GO}	0.9	K_{GO}	2.7
I_{BO}	3.0	K_{BO}	0.14

The values for the inertias and spring constants listed in Fig. 8 are in some cases quite rough estimates as they are computed on the basis of simplified geometries and lumped masses. An angular momentum value of 450 ft-lb-sec was assumed for this analysis. The resulting asymptotic gain vs frequency plot for $\dot{\theta}_{TT}/T_M$ is shown in Fig. 9. For comparison, the noncompliant (infinite stiffness) case is also plotted as a dashed line, given by

$$\dot{\theta}_{TT}/T_M = 1/I_G s \tag{15}$$

where I_G is the total rotating inertia in the input axis, given by

$$I_G = I_{TT} + I_{GI} + I_{WI} \approx 2.1 \text{ ft-lb-s}^2 \tag{16}$$

At low frequencies, the inertia has effectively increased to the value

$$I_{GE} = I_G + H^2\left(\frac{1}{K_{WO}} + \frac{1}{K_{GO}} + \frac{1}{K_{BO}}\right) \approx 3.7 \text{ ft-lb-s}^2 \tag{17}$$

At higher frequencies, the effect of the compliances is to increase the gain significantly above the rigid-body case as is shown. Some of the break frequencies can be quite closely related to specific springs and inertias; a few relations are shown in the figure (I_O denotes total inertia in the output axis). Since the damping ratios of compliance modes are normally very light, the gains at these frequencies are considerably greater than is shown by the asymptotic plot in the figure. Table 2 gives the additional gain that exists at a resonance for selected values of ζ. Values for ζ have not been determined, but are typically less than 0.1 for the structures used in the CMG. Since the

Table 2 Additional gain vs ζ at resonant modes

ζ	M_m	dB
0.1	5	14
0.05	10	20
0.02	25	28
0.01	50	34

phase lag for the given response remains between $\pm 90°$ for all frequencies, high gains at the resonances would not cause instability if there were no other sources of phase lag in the control loop. But since the torquer current loop, the tachometer, and amplifiers introduce phase lag, it is necessary to generally maintain the loop gain below zero dB at higher frequencies.

Consider the application of the proportional-plus-integral control law with $K_I = 10{,}000$ ft-lb/rad for low-level performance, and with

$$K_P = 2\zeta(K_I I_{GE})^{1/2} = 272 \text{ ft-lb-s} = 48.7 \text{ dB above 1 ft-lb-s} \tag{18}$$

for $\zeta = 0.7$. The frequency plot for this control law (T_{MC}/θ_E) is also shown in Fig. 9 with the amplitude scale on the right-

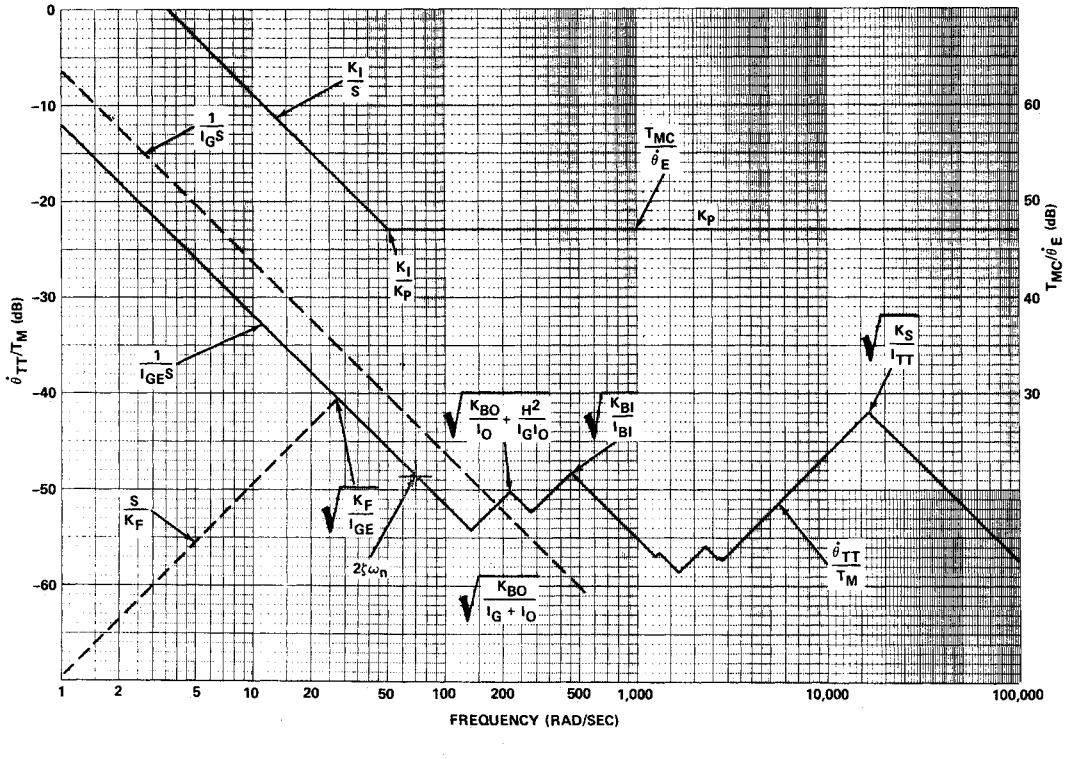

Fig. 9 Frequency response for higher-order compliant model.

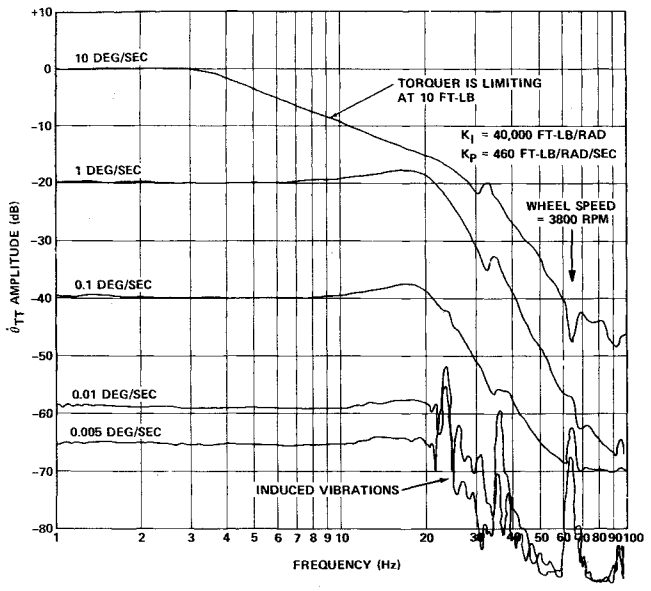

Fig. 10 Gimbal-rate frequency response demonstrated.

hand side. The resulting gimbal control system bandwidth (with the prefilter) is

$$\omega_n = (K_I/I_{GE})^{1/2} = 52 \text{ rad/s} = 8.3 \text{ Hz} \quad (19)$$

and the crossover frequency is

$$2\zeta\omega_n = 73 \text{ rad/s} = 11.6 \text{ Hz} \quad (20)$$

When the control-law gain is added to the gain of the gimbal dynamics, the open-loop gain is much greater than zero dB at the resonant frequencies. A considerable amount of additional filtering is therefore required to reduce the gain, and adequate frequency separation between the crossover frequency and the resonant frequencies must be provided for such filtering. The guideline of Eq. (14) provides such frequency separation when K_O is the over-all output axis stiffness.

Demonstrated Performance

Application of the above principles resulted in a demonstration of wide bandwidth control of gimbal rate at lower levels than previously believed possible for large CMGs. This demonstration was accomplished in July 1972 as part of a technical effort on CMGs directed at the High Energy Astronomical Observatory (HEAO). Figure 10 shows the frequency response curves obtained. At the gimbal rate of 0.005°/sec, which is slower than the hour hand of a clock (0.0083°/sec), and at a frequency of 20 Hz (125 rad/sec) the angular displacement of the gimbal is only 0.144 arc-sec, well within the spring region of the gimbal friction profile (see Fig. 4). This performance was demonstrated both with the wheel standing still and running to show that wheel-induced dither is not required to obtain the low-level performance. Figure 10 shows the case where the wheel was running.

The demonstration was performed with the CMG mounted on a rigid pedestal with control system components and electronics under development for the HEAO program. The direct-drive brushless d.c. torquer and the brush-type d.c. tachometer of the gimbal-rate control loop were mounted in close proximity on one end of the gimbal axis (near side as shown in Fig. 1).

The gimbal rate which is plotted in the figures was measured by a completely separate precision tachometer mounted on the opposite end of the gimbal axis from the module that houses the torquer and the control tachometer. The precision tachometer, totally independent of the control loop, gave positive indication that the rate of the controlled torquer-tachometer rotor was transmitted to the gimbal. The rate of the wheel about the input axis is not directly measurable, but with knowledge of the stiffness of the structure between the gimbal shaft and the wheel rim in the output axis, it can be analytically demonstrated that the wheel responds. Insufficient stiffness in this structure would become evident in the frequency response characteristics and would complicate or prevent stabilization of the loop at the high integral gain (40,000 ft-lb/rad) used in the demonstration. It was therefore concluded that the precision tachometer gave an accurate indication of the angular rate of the wheel about the gimbal axis.

A Note on Double-Gimbal CMGs

Double-gimbal CMGs can be controlled similarly to single-gimbal CMGs; that is, they can be gimbal-rate controlled to produce output torque in an orthogonal axis. They can also be torque-controlled to yield output torque directly in the gimbal axis by permitting the gyro to precess in the orthogonal axis. In the latter case, low-level performance is severely limited by the dynamic range of the gimbal torquer which is typically no better than 50:1. If gimbal-rate control is used for a double-gimbal CMG, the output torque is transmitted through the output axis gimbal torquer (orthogonal to the gimbal axis where rate is commanded), and the output-axis stiffness is then equal to the integral gain of that gimbal control loop. The guideline given by Eq. (14) can therefore not be met with a double-gimbal CMG, since both gimbal axes serve as both input and output axes. It is pointed out, however, that this guideline has not been proved to be an absolute requirement. The greater damping possible in the stiffness provided by a control loop in comparison with mechanical structures might permit violation of this guideline for double-gimbal CMGs, although this has not been demonstrated.

Conclusions

The performed analyses and hardware tests have led to the following two guidelines for obtaining extremely precise control of gimbal rate in a CMG: a) the control-loop integral gain should be substantially higher than the gimbal friction spring constant; and b) the stiffness of the structures between the CMG rotor and the spacecraft about the output axis should be substantially higher than the integral gain of the control loop.

These guidelines point to hardware development for reducing the gimbal friction spring constant K_F. By reducing this stiffness, the integral gain K_I can be reduced in proportion as long as it remains high enough for the required bandwidth. Reduction in K_F can be achieved by: a) replacing the brush-type tachometer with a brushless type, b) designing the torquer for minimum hysteresis and cogging torques (at a cost in weight), c) designing the brush springs (in sliprings and brush-type tachometer) to be compliant, d) selecting the gimbal bearings and/or bearing lubrication on the basis of reduced K_F, if possible, and e) reducing the radius of all friction-producing components where possible.

Also, if the gimbal freedom can be allowed to be limited to, say, two revolutions, the sliprings can be replaced with flexible leads to potentially reduce K_F.

References

[1] Hartter, L. L., Ryback, S. C., Mayo, R. A., and Yeichner, J. A., "A Hard-Mounted Ultrahigh-Accuracy Pointing Control System," AIAA Paper 72-854, Stanford, Calif., 1972.

[2] Ryback, S. C., Lieberman, S. I., Hartter, L. L., Gregory, R. L., and Nakashima, A. K., "Achieving Ultrahigh Accuracy with a Body Pointing CMG/RW Control System," AIAA Paper 73-883, Key Biscayne, Fla., 1973.

[3] Osborne, N. A., "Fine Pointing Improvement by Augmentation Methods," AIAA Paper 73-868, Key Biscayne, Fla., 1973.

[4] Dahl, P. R., "A Solid Friction Model," Rept. TOR-0158 (3107-18)-1, May 1968, The Aerospace Corp., El Segundo, Calif.